Folding of the triangular lattice with quenched random bending rigidity

P. Di Francesco, E. Guitter, and S. Mori*
Service de Physique Théorique, C.E.A. Saclay, F-91191 Gif-sur-Yvette Cedex, France
(Received 19 July 1996)

We study the problem of folding of the regular triangular lattice in the presence of a quenched random bending rigidity $\pm K$ and a magnetic field h (conjugate to the local normal vectors to the triangles). The randomness in the bending energy can be understood as arising from a prior marking of the lattice with quenched creases on which folds are favored. We consider three types of quenched randomness: (i) a ''physical'' randomness where the creases arise from some prior random folding; (ii) a Mattis-like randomness where creases are domain walls of some quenched spin system; (iii) an Edwards-Anderson-like randomness where the bending energy is $\pm K$ at random, independently on each bond. The corresponding (K,h) phase diagrams are determined in the hexagon approximation of the cluster variation method. Depending on the type of randomness, the system shows essentially different behaviors. [S1063-651X(97)08001-X]

PACS number(s): 05.50.+q, 64.60.−i, 82.65.Dp

I. INTRODUCTION

The statistical properties of polymerized membranes, or tethered surfaces, have been widely discussed in the past few years [1–3]. A polymerized membrane is the two-dimensional generalization of a linear polymer [1–4]. Its energy involves both an in-plane elastic (strain) contribution and an out-of-plane (bending) one. At low temperature, such a membrane with bending rigidity is asymptotically flat and its radius of gyration R_G increases as the linear internal dimension L of the surface [5–10]. As a function of temperature, the membrane without self-avoiding interaction (phantom membrane) undergoes a crumpling transition from the low-temperature flat phase to a high-temperature crumpled phase ($R_G \sim \sqrt{\ln L}$) [11,12]. The mechanism of the transition, in particular the stability of the flat phase, is rather subtle and relies on the coupling between in-plane and out-of-plane deformation modes [5].

Very generally, two-dimensional (2D) membranes can be discretized into triangulations, whose faces are endowed with natural Heisenberg spin variables, representing the direction of the local normal vector to the surface [1]. Polymerized membranes, which have a fixed connectivity, then translate into statistical spin systems on the *regular* triangular lattice. The corresponding spin system is, however, involved because the resulting spins are not independent variables. The constraint of being normal vectors to a surface causes a long-range interaction between the spins, which stabilizes the ordered flat phase, as opposed to the case of the usual two-dimensional unconstrained Heisenberg model, always disordered [1,5].

The above mechanism clearly indicates the subtlety of the correspondence between geometrical objects and spin systems, especially in two dimensions. In order to understand this, several simple models have been proposed. The simplest one is probably a square lattice model introduced by David and Guitter [7]. The model is a discrete rigid bond square lattice, which is allowed to fold onto itself along its bonds in a two-dimensional embedding space. The constraint there makes the folds propagate along straight lines. In the presence of bending rigidity, the system is always flat.

A triangular lattice version of this 2D folding model was then introduced by Kantor and Jarić [13]. Describing the (up or down) normal to each triangle by a spin variable $\sigma = \pm 1$, the model Hamiltonian translates into that of the Ising model with, however, constraints on the spin variables. This results in several new features, and a totally new phase diagram, as compared with the usual Ising model [13–16]. Finally, the folding of the triangular lattice embedded in a three-dimensional discrete space has been formulated as a 96-vertex model [17,18].

Constraints do not appear only in the physical degrees of freedom, like local normal vectors. If the membrane has disorder, the disorder itself can also be constrained in some cases. For example, if one folds a piece of paper and makes a crease, this will generate a spontaneous curvature along the crease. If one now crumples the paper randomly by hand [4,19], the generated spontaneous curvature will be directly related to the configuration of the normal vectors of the resulting crumpled configuration. For the latter to be accepted as a physical configuration, the normal vectors should also obey some constraints. The induced disorder (in this case the induced random spontaneous curvature) should thus obey similar ''physical'' constraints.

Here we study a simple model of folding with such a ''physical'' quenched randomness. As a model, we use the triangular lattice folded in two dimensions, with a quenched random bending rigidity arising from a first random prefolding process. As our main result, we find a transition to a low-temperature frozen phase where the lattice is preferentially trapped into the original random prefolded state. In order to clarify the importance of the ''physical'' constraints on the disorder, we then study two other types of disorder distributions where the random bending rigidity cannot, in general, be realized by any particular random prefolding process. In such a case, a frustration is created in the sense that the bending energy cannot be trivially minimized by any folded state of the lattice. In the absence of any other exter-

*Present address: Dept. of Physics, Graduate School of Science, University of Tokyo, Hongo 7-3-1, Bunkyo-ku, Tokyo 113, Japan.

nal field, we find that the system is unable to develop a frozen phase in this case.

The paper is organized as follows. In Sec. II, we first discuss the general folding problem of the triangular lattice and recall some known facts about it. We then describe the precise type of ''physical'' randomness that we consider on the lattice and which we write as a Mattis-like spin system [20] with constraints. In Sec. III, we describe the cluster variation method that we shall apply to the study of the thermodynamics of the system [21–23]. We first describe the procedure for a general disordered system. We then restrict ourselves to the hexagonal approximation in which the clusters are made of a maximum of six triangles. Next, we analyze the pure (without disorder) system again, as a particular limiting case with trivial disorder. The results for the fully disordered system, and in particular the transition to a frozen phase, are presented in Sec. IV. After giving a few results following from a reduced variable analysis, we present the complete phase diagram of the system. In Sec. V, we study two other variants of the disorder. In particular, we discuss the specificity of the ''physical'' constraint on the random bending rigidity. We present for each type of disorder the corresponding phase diagram. Some concluding remarks are gathered in Sec. VI.

II. FOLDING WITH QUENCHED RANDOM BENDING RIGIDITY

In this section, we first recall the rules of folding for the triangular lattice [13]. We then introduce disorder in the problem in terms of a *random bending rigidity*.

A. Folding of the triangular lattice: pure case

Let us consider a regular triangular lattice that can be folded onto itself along its bonds. We allow only for complete foldings which result in *two-dimensional* folded configurations. Each bond thus serves as a hinge between its two neighboring triangles and is in either one of the two states: folded (with the two neighboring triangles face to face) or not (with the two neighboring triangles side by side). A folded state of the system is entirely determined by the list of its folded bonds. In this definition, the folding process may cause self-intersections and the model corresponds to a ''phantom'' membrane. Also this does not distinguish between the different ways of folding that result in the same folded state.

One can easily see that, among the 2^6 possible fold configurations for the six bonds surrounding a given vertex, only 11 states are allowed, corresponding to actual foldings of the surrounding hexagon [13]. These configurations are displayed in Fig. 1. It can be checked that imposing everywhere one of these eleven local environments is sufficient to define the folding consistently throughout the lattice. The folding of the triangular lattice is thus simply expressed as an 11-vertex model on the lattice. Note that, even if the folding is defined locally, its nature is highly nonlocal. Since all vertices in Fig. 1 have an even number of elementary folds, these folds form folding lines without end points. Moreover all ''folded'' vertices [vertices (b)–(k) in Fig. 1] have at least one fold on the left half of the hexagon and one on the right. Thus folds are forced to propagate through the entire lattice [14].

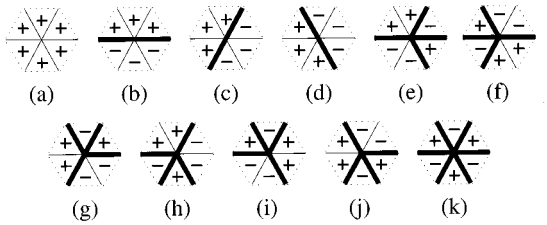

FIG. 1. The 11 local fold environments for a vertex. Folds are represented by thick lines. One of the two (opposite) possible spin configurations on the triangles is also indicated.

Folding can also be expressed with spin variables $\sigma_i=\pm 1$ living on the elementary triangles, which indicate whether the ith triangle faces up or down in the folded state. The spin variable changes its sign between two neighboring triangles, if and only if their common bond is folded, i.e., folding lines are domain walls of the spin system. One can think of the spin as the normal vector to the triangle. We depict the corresponding spin configurations on Fig. 1. Note that there are two spin configurations for each folded state, due to the degeneracy under reversal of all spins.

Clearly, the only allowed vertex environments are those with exactly zero, three, or six surrounding up spins. In other words, for a spin configuration to correspond to a folded state, the six spins σ_i $(i=1,2,...,6)$ around any vertex v must satisfy the *local constraint* [14]

$$\Sigma_v \equiv \sum_{i \text{ around } v} \sigma_i = 0 \mod 3, \tag{2.1}$$

since $\Sigma_v=2$ (number of up spins) $-$ 6 is a multiple of 3 if and only if the number of up spins itself is a multiple of 3. Folding is thus expressed here as a *constrained Z_2 spin system*.

The statistical behavior of this system has been extensively studied, using a transfer-matrix formalism [13,15], the correspondence with a solvable three-coloring model [14] and a cluster variation method [16]. Introducing a bending energy term $-J\sigma_i\sigma_j$ between nearest neighbors and a magnetic field term $-H\sigma_i$, the following model Hamiltonian was considered:

$$\mathcal{H}_{\text{Ising}} = -J\sum_{(ij)} \sigma_i\sigma_J - H\sum_i \sigma_\iota . \tag{2.2}$$

This is nothing but the Ising Hamiltonian, which is here, however, coupled to the local constraint (2.1). In the folding context, the magnetization simply measures the projected area of the lattice (i.e., the algebraic area of the domain enclosed by its boundary) and the magnetic field can thus be interpreted as a lateral tension term. For convenience we will use the reduced coupling and magnetic field

$$K \equiv J/k_BT, \quad h \equiv H/k_BT. \tag{2.3}$$

The phase diagram of the system is shown in Fig. 2. In order to characterize each phase, two order parameters are introduced. One is the usual magnetization,

$$M = \frac{1}{N_t}\left\langle \left(\sum_{\triangle} \sigma_i + \sum_{\triangledown} \sigma_i \right) \right\rangle, \tag{2.4}$$

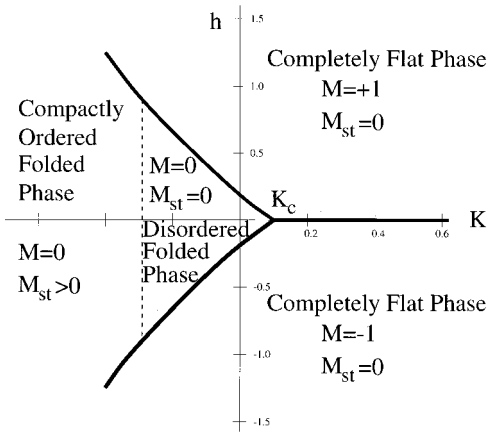

FIG. 2. Phase diagram in the (K,h) plane. Three first-order lines $h=h_c(K)$, $-h_c(K)$ $(K<K_c)$, and $h=0$ $(K>K_c)$ separate the three phases $M=0$, ± 1 and meet at the triple point $(K_c,0)$. The dashed line represents the transition line between the disordered folded phase $M=0$, $M_{\rm st}=0$, and the compactly ordered folded phase $M=0$, $M_{\rm st}\neq 0$.

and the other is the staggered magnetization

$$M_{\rm st}=\frac{1}{N_t}\left\langle\left(\sum_{\triangle}\sigma_i-\sum_{\triangledown}\sigma_i\right)\right\rangle, \tag{2.5}$$

where the sum is performed separately on triangles pointing up and down, dividing the original triangular lattice into two interpenetrating sublattices. Here N_t is the total number of triangles in the system. Three phases exist: a completely flat phase ($M=\pm 1$, $M_{\rm st}=0$), a disordered folded state ($M=0$, $M_{\rm st}=0$), and a compactly ordered folded state ($M=0$, $M_{\rm st}\neq 0$) [15,16]. Note that the flat phase has a maximal magnetization $|M|=1$ and is indeed frozen in the pure completely flat state with all spins aligned. There is no flat phase with intermediate $(0<|M|<1)$ magnetization. Three first-order transition lines $h=h_c(K)$, $-h_c(K)$ $(K<K_c)$, and $h=0(K>K_c)$ separate the three phases $M=0$, ± 1, with a triple point at $K_c\sim 0.1$ (estimated from either the transfer matrix [15] or the cluster variation [16] approach). For negative K, the transition between the disordered folded phase and a compactly ordered (antiferromagnetic) folded phase with staggered order parameter $M_{\rm st}\neq 0$ is found to be continuous at $h=0$ [16]. This transition is represented by the broken line of Fig. 2, which intersects the horizontal $(h=0)$ axis at $K\sim -0.284$. We see here that, when compared with the usual unconstrained Ising model, the phase diagram has been strongly modified. In particular, it is now asymmetric with respect to K with the usual continuous ferromagnetic transition replaced by an abrupt first-order transition to a completely ordered phase.

B. Quenched random bending rigidity

What kind of disorder should one introduce in the above model [Eq. (2.2)]? Since we are dealing with folding of a phantom object with a two-dimensional resulting folded state, we cannot distinguish between $\pm 180°$ folds, thus we cannot introduce any spontaneous curvature term. Disorder will appear here in the form of a random bending rigidity K_{ij}. The most general Hamiltonian with random nearest-neighbor coupling K_{ij} and a constant external field h is (we drop the k_BT factor, thus using reduced coupling constants)

$$\mathcal{H}_{\rm random}=\sum_{(ij)}-K_{ij}\sigma_i\sigma_j-h\sum_i\sigma_i. \tag{2.6}$$

There are several possible choices for K_{ij}. One possibility is the Edwards-Anderson model for spin glasses [24], where $K_{ij}=\pm K$ independently on each bond. Such a model is interesting as it may have a spin-glass phase. In such a phase, spins are randomly oriented ($M=0$ and $M_{\rm st}=0$), but the following order parameter q takes a nonzero value:

$$q=\frac{1}{N_t}\sum_i\overline{\langle\sigma_i\rangle^2}. \tag{2.7}$$

Here the overbar stands for the quenched average over the randomness. We shall discuss this type of disorder in Sec. V.

As has been discussed in the Introduction, we are interested in another type of ''physical'' disorder where the random bending rigidity has been generated by a prior irreversible folding of the lattice [4,19]. We have in mind the picture of a crumpled piece of paper marked with irreversible creases. The effect of this irreversible crumpling is to impose the corresponding crumpled state as the new ground state of the system. No frustration will occur as long as one does not strain the paper. The model Hamiltonian should thus have that crumpled state as its ground state and this information should be included in K_{ij}. One natural choice for K_{ij} with a ''random'' ordered phase and no frustration is that of a Mattis model [20]. In this model, the bending rigidities K_{ij} are functions of a set of random face variables τ_i:

$$K_{ij}=K\tau_i\tau_j. \tag{2.8}$$

The $\tau_i=\pm 1$ are ''frozen'' according to a specified probability distribution $\rho_\tau(\tau_1,\tau_2,\ldots,\tau_{N_t})$ reminiscent of the first irreversible crumpling process. The total Hamiltonian is then given by

$$\mathcal{H}_{\rm Mattis}=-K\sum_{(ij)}\tau_i\tau_j\sigma_i\sigma_j-h\sum_i\sigma_i. \tag{2.9}$$

As is well known, if there is no constraint on spin variables, the gauge transformation

$$\sigma_i'\rightarrow\sigma_i\tau_i \tag{2.10}$$

makes the above model Eq. (2.9) in zero external field $h=0$ equivalent to the pure system [20]. At $K=\infty$, the state with $\sigma_i=\tau_i$ is recovered as the ground state.

In our model, the spin variables are constrained by Eq. (2.1) and the above gauge transformation cannot be performed since it does not preserve the folding constraint. Moreover, the ground state $\sigma_i=\tau_i$ can be reached only if the τ variables themselves obey the folding constraint:

$$\sum_{i\ \text{around}\ v}\tau_i=0\mod 3. \tag{2.11}$$

This type of τ configuration is what we call a ''physical'' disorder. We shall restrict ourselves to this type of disorder in Secs. III and IV. We will return to other types of disorder (such as the Edwards-Anderson model) later in Sec. V.

From the above discussion, we understand the physical origin of the local constraint on the τ variables. Then what probability distribution $\rho_\tau(\tau_1,\tau_2,\ldots,\tau_{N_t})$ should we use for them? Since the τ variables obey the same constraint as the pure σ system described in the first part of this section, we can take advantage of the solution of this pure system by simply assuming that the τ distribution is described by a particular (appropriately chosen) point in the disordered phase of the phase diagram of Fig. 2. A natural choice is the point at the origin of the phase diagram ($K=h=0$) since it then does not involve any energy parameter for the disorder and treats as equiprobable all allowed configurations of ''physical'' disorder. In other words, we shall take for the distribution $\rho_\tau(\tau_1,\tau_2,\ldots,\tau_{N_t})$ the density of the pure constrained problem at $K=h=0$. Due to the constraint, this density remains nontrivial.

III. CLUSTER VARIATION METHOD FOR THE DISORDERED SYSTEM

In this section we explain in detail the hexagon approximation of the cluster variation method (CVM) generalized to a random system [21–23]. In Sec. III A, we explain the method in the general case. In Sec. III B, we apply the CVM to the pure system ($K_{ij}=K$) as a limiting case with trivial disorder. As mentioned above, this is also instrumental to give an explicit form for ρ_τ, which is necessary to tackle the fully disordered case. We also discuss several symmetry breakings of the model.

A. The CVM and its hexagon approximation

The CVM is a closed-form approximation based on the minimization of an approximated free-energy density functional, which is obtained by a truncation of the cluster expansion of the full free-energy density functional appearing in the exact variational formulation of the problem [25,26]. Consider our spin system σ_i with N_t sites and Hamiltonian (2.6) [23]. The configuration of the random bond couplings K_{ij} is specified by a probability distribution $P(\{K_{ij}\})$. In our case of ''physical'' disorder where $K_{ij}=K\tau_i\tau_j$, we shall have

$$P(\{K_{ij}=K\tau_i\tau_j\})=\rho_\tau(\tau_1,\ldots,\tau_{N_t}). \tag{3.1}$$

The discussion below is, however, more general.

In terms of a density matrix $\rho(\sigma_1,\sigma_2,\ldots,\sigma_{N_t}|\{K_{ij}\})$ for each configuration $\{K_{ij}\}$, we define the variational free energy associated with the Hamiltonian $\mathcal{H}_{\rm random}(\sigma,\{K_{ij}\})$ (from now on, we use the notation $\sigma=\{\sigma_i\}$) as

$$\mathcal{F}(\{K_{ij}\})=\left[\sum_\sigma \rho(\sigma|\{K_{ij}\})[\mathcal{H}_{\rm random}(\sigma,\{K_{ij}\}) + \ln\rho(\sigma|\{K_{ij}\})]\right]_{\rm min}. \tag{3.2}$$

The subscript min means that the above expression must be taken at its minimum with respect to $\rho(\sigma|\{K_{ij}\})$. This is the well-known variational principle. The minimization is performed at fixed $\{K_{ij}\}$ with the normalization constraint:

$$\sum_\sigma \rho(\sigma|\{K_{ij}\})=1. \tag{3.3}$$

The quenched free-energy $\mathcal{F}$ is then given by

$$\mathcal{F}=\sum_{\{K_{ij}\}} P(\{K_{ij}\})\mathcal{F}(\{K_{ij}\}), \tag{3.4}$$

where the sum extends over all possible realizations of the disorder. Upon introducing the generalized density matrix

$$\rho(\sigma,\{K_{ij}\})=P(\{K_{ij}\})\rho(\sigma|\{K_{ij}\}), \tag{3.5}$$

one can easily show that

$$\mathcal{F}=\left[\sum_{\sigma,\{K_{ij}\}} \rho(\sigma,\{K_{ij}\})[\mathcal{H}_{\rm random}(\sigma,\{K_{ij}\}) + \ln\rho(\sigma,\{K_{ij}\})]\right]_{\rm min}+S_{\rm Dis} \tag{3.6}$$

where the minimization is now on a density $\rho(\sigma,\{K_{ij}\})$ for both σ and $\{K_{ij}\}$ with the constraint

$$\sum_\sigma \rho(\sigma,\{K_{ij}\})=P(\{K_{ij}\}). \tag{3.7}$$

The quantity $S_{\rm Dis}$ is a constant term depending only on the probability distribution for the disorder and reads

$$S_{\rm Dis}=-\sum_{\{K_{ij}\}} P(\{K_{ij}\})\ln P(\{K_{ij}\}). \tag{3.8}$$

In such a scheme it can be shown that the quenched average of the expectation value $\langle A(\sigma,\{K_{ij}\})\rangle$ of an operator $A(\sigma,\{K_{ij}\})$ is given by

$$\overline{\langle A(\sigma,\{K_{ij}\})\rangle}=\sum_{\{K_{ij}\}} P(\{K_{ij}\})\langle A(\sigma,\{K_{ij}\})\rangle = \sum_{\{K_{ij}\},\sigma} \rho_{\rm min}(\sigma,\{K_{ij}\})A(\sigma,\{K_{ij}\}), \tag{3.9}$$

where $\rho_{\rm min}(\sigma,\{K_{ij}\})$ is the density at the minimum of the quenched free-energy functional (3.6).

The CVM is obtained by taking the thermodynamic limit $N_t\to\infty$ and truncating the cumulant expansion for the entropy $\mathcal{S}\equiv-\Sigma_{\sigma,\{K_{ij}\}}\rho(\sigma,\{K_{ij}\})\ln\rho(\sigma,\{K_{ij}\})$ appearing in Eq. (3.6) to a set of ''maximal preserved clusters'' Γ_i, $i=1,2,\ldots,r$ (and all their translated images). The variational principle will then be applied to the reduced density matrix $\rho_{\Gamma_i}(\sigma,\{K_{ij}\})$ associated with the maximal preserved clusters Γ_i, i.e., the minimization will be performed on this reduced set of densities.

In the hexagon approximation for the triangular lattice, the largest clusters appearing in the expansion are hexagons. Hereafter we restrict our presentation to the case of the

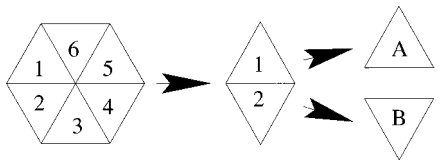

FIG. 3. Labeling of the spins on an elementary hexagon. Each site i $(=1,...,6)$ supports a spin variable σ_i and a disorder variable τ_i. The reduction process from ρ_6 to ρ_2 and to $\rho_{1A(B)}$ is also indicated.

Mattis-like coupling $K_{ij}=K\tau_i\tau_j$. For the other cases, the generalization is straightforward. We introduce the reduced density matrix for a hexagon:

$$\rho_6(\sigma_1,\sigma_2,\sigma_3,\sigma_4,\sigma_5,\sigma_6,\tau_1,\tau_2,\tau_3,\tau_4,\tau_5,\tau_6). \tag{3.10}$$

The spins in the argument of ρ_6 follow each other counterclockwise in the hexagon, and the first one is on the A sublattice (see Fig. 3), i.e., is pointing up. This reduced density matrix represents the probability for one hexagon to have fixed values of σ and τ. It is normalized according to

$$\sum_{\{\sigma\}} \rho_6(\{\sigma\},\{\tau\})=\rho_{\tau,6}(\{\tau\}), \tag{3.11}$$

where $\rho_{\tau,6}$ is the six-point probability for the disorder variable on a hexagon as obtained from the corresponding partial trace of $\rho_\tau(\tau_1,\ldots,\tau_{N_t})$ in the thermodynamic limit. We assume that this six-point reduced density is the same for each hexagon, i.e., that the distribution of disorder is translationally invariant.

We also introduce the site and pair density matrices $\rho_{1A(B)}(\sigma_1,\tau_1)$, $\rho_2(\sigma_1,\sigma_2,\tau_1,\tau_2)$, which are defined as symmetrized partial traces of ρ_6 by

$$\begin{aligned}
&\rho_2(\sigma_1,\sigma_2,\tau_1,\tau_2)\\
&\quad\equiv\tfrac{1}{6}\sum_{\substack{\sigma_3,\sigma_4,\sigma_5,\sigma_6\\ \tau_3,\tau_4,\tau_5,\tau_6}}\\
&\qquad\times[\rho_6(\sigma_1,\sigma_2,\sigma_3,\sigma_4,\sigma_5,\sigma_6,\tau_1,\tau_2,\tau_3,\tau_4,\tau_5,\tau_6)\\
&\qquad+\rho_6(\sigma_3,\sigma_2,\sigma_1,\sigma_4,\sigma_5,\sigma_6,\tau_3,\tau_2,\tau_1,\tau_4,\tau_5,\tau_6)\\
&\qquad+\rho_6(\sigma_3,\sigma_4,\sigma_1,\sigma_2,\sigma_5,\sigma_6,\tau_3,\tau_4,\tau_1,\tau_2,\tau_5,\tau_6)\\
&\qquad+\rho_6(\sigma_3,\sigma_4,\sigma_5,\sigma_2,\sigma_1,\sigma_6,\tau_3,\tau_4,\tau_5,\tau_2,\tau_1,\tau_6)\\
&\qquad+\rho_6(\sigma_3,\sigma_4,\sigma_5,\sigma_6,\sigma_1,\sigma_2,\tau_3,\tau_4,\tau_5,\tau_6,\tau_1,\tau_2)\\
&\qquad+\rho_6(\sigma_1,\sigma_3,\sigma_4,\sigma_5,\sigma_6,\sigma_2,\tau_1,\tau_3,\tau_4,\tau_5,\tau_6,\tau_2)],\\
&\rho_{1A}(\sigma_1,\tau_1)\equiv\sum_{\sigma_2,\tau_2}\rho_2(\sigma_1,\sigma_2,\tau_1,\tau_2),\\
&\rho_{1B}(\sigma_2,\tau_2)\equiv\sum_{\sigma_1,\tau_1}\rho_2(\sigma_1,\sigma_2,\tau_1,\tau_2).
\end{aligned} \tag{3.12}$$

Here we have introduced two site density matrices, ρ_{1A} and ρ_{1B}, corresponding to the two interpenetrating sublattices in which the triangular lattice can be divided (see Fig. 3).

After the appropriate truncation of the cumulant expansion of $\mathcal{S}$ at the level of hexagonal clusters, we get the approximate CVM quenched free energy per hexagon as a functional of $\rho_6(\{\sigma_i\},\{\tau_i\})$ only [by implicit use of Eq. (3.12)] [25],

$$\begin{aligned}
f(\rho_6(\{\sigma_i\},\{\tau_i\}))=&-3K\ \mathrm{Tr}_{\sigma,\tau}[\tau_1\tau_2\sigma_1\sigma_2\rho_2(\sigma_1,\sigma_2,\tau_1,\tau_2)]\\
&-h\ \mathrm{Tr}_\sigma[\sigma_1\rho_{1A}(\sigma_1,\tau_1)]\\
&-h\ \mathrm{Tr}_\sigma[\sigma_2\rho_{1B}(\sigma_2,\tau_2)]+\mathrm{Tr}_{\sigma,\tau}(\rho_6\ln\rho_6)\\
&-3\ \mathrm{Tr}_{\sigma,\tau}(\rho_2\ln\rho_2)+\mathrm{Tr}_{\sigma,\tau}(\rho_{1A}\ln\rho_{1A})\\
&+\mathrm{Tr}_{\sigma,\tau}(\rho_{1B}\ln\rho_{1B})+\mathrm{Tr}_\tau\{\lambda_\tau(\{\tau_i\})\\
&\times[\mathrm{Tr}_\sigma\rho_6(\{\sigma_i\},\{\tau_i\})-\rho_{\tau,6}(\{\tau_i\})]\}+S_\tau,
\end{aligned} \tag{3.13}$$

to be minimized with respect to $\rho_6(\{\sigma_i\},\{\tau_i\})$. [The cumulant expansion of the entropy can be understood as follows. We write the truncated entropy as

$$\mathcal{S}=\sum_{\text{hexagons }H}\mathcal{S}_H-\sum_{\text{pairs }P}\mathcal{S}_P+\sum_{\text{triangles }T}\mathcal{S}_T,$$

where we must first subtract the contribution of pairs of neighboring triangles and readd that of single triangles to avoid overcounting. Noting that the numbers N_H, N_P, N_{TA}, and N_{TB} of, respectively, hexagons, pairs and triangles of the sublattices A and B satisfy $N_P/N_H=3$, $N_{TA}/N_H=N_{TB}/N_H=1$, this leads to the entropy per hexagon appearing in Eq. (3.13).] Here Tr stands for trace and $\lambda_\tau(\{\tau_i\})$ are Langrange multipliers that ensure the normalization of $\rho_6(\{\sigma_i\},\{\tau_i\})$, according to Eq. (3.11). S_τ is the entropy for the disorder variable τ_i, for which we also use the CVM estimate:

$$S_\tau=\mathrm{Tr}_\tau(\rho_{\tau,6}\ln\rho_{\tau,6})-3\ \mathrm{Tr}_\tau(\rho_{\tau,2}\ln\rho_{\tau,2})+2\ \mathrm{Tr}_\tau(\rho_{\tau,1}\ln\rho_{\tau,1}), \tag{3.14}$$

where $\rho_{\tau,2}$ and $\rho_{\tau,1}$ are partial (symmetrized) traces of $\rho_{\tau,6}$. With the above definitions, our free energy can be regarded as a function of ρ_6 only and taking the derivative with respect to a generic element of ρ_6 we find the stationarity conditions

$$\begin{aligned}
&\rho_6(\{\sigma_i\},\{\tau_i\})\\
&\quad=\exp\left[-\lambda_\tau(\{\tau_i\})+\frac{K}{2}\sum_{i=1,6}\tau_i\tau_{i+1}\sigma_i\sigma_{i+1}+\frac{h}{3}\sum_{i=1,6}\sigma_i\right]\\
&\qquad\times[\rho_2(\sigma_1,\sigma_6,\tau_1,\tau_6)\rho_2(\sigma_1,\sigma_2,\tau_1,\tau_2)\\
&\qquad\times\rho_2(\sigma_3,\sigma_2,\tau_3,\tau_2)\rho_2(\sigma_3,\sigma_4,\tau_3,\tau_4)\\
&\qquad\times\rho_2(\sigma_5,\sigma_4,\tau_5,\tau_4)\rho_2(\sigma_5,\sigma_6,\tau_5,\tau_6)]^{1/2}\\
&\qquad\times[\rho_{1A}(\sigma_1)\rho_{1B}(\sigma_2)\rho_{1A}(\sigma_3)\rho_{1B}(\sigma_4)\\
&\qquad\times\rho_{1A}(\sigma_5)\rho_{1B}(\sigma_6)]^{-1/3},
\end{aligned} \tag{3.15}$$

with the convention $\sigma_7=\sigma_1$, $\tau_7=\tau_1$.

One can solve this set of equations with the definitions of Eqs. 3.12 and the normalization constraint (3.11) by the so-

called natural iteration method [21]. Starting from some assumption on ρ_2 and iterating the above equation, ρ_6 converges to a solution of Eq. (3.15) which is moreover a local *minimum* of the approximate free energy (3.13). To find a global minimum, it is in general necessary to start the iteration with different sets of initial conditions on ρ_2 appropriately chosen to reach the different expected phases. At each step, the normalization condition (3.11) is recovered by adjusting the Lagrange multiplier for each realization of the disorder on the hexagon. Before going to the analysis of the model with disorder, in Sec. III B we will revisit the pure case [16]. One reason is that we need to fix the probability distribution for the disorder variables $\rho_\tau(\{\tau_i\})$.

B. Pure case and explicit form for ρ_τ

In this section, we reconsider the pure case for $h=0$ in detail within the CVM approximation as a particular trivial realization of disorder where all K_{ij} are constant and equal to K [16]. We only need to consider the ''pure'' six-point functions $\rho_6(\sigma_i)$, which do not depend on the τ_i variable any longer. We can easily recognize that the $2\times 11=22$ elements of ρ_6, which correspond to the weights for each state in Fig. 1, are not all independent since some of the states are related by simple symmetries and should thus have the same weight. This of course assumes that the corresponding symmetries are not spontaneously broken. Hereafter we only consider the system for $h=0$ and consider three types of solutions corresponding to the three different symmetries of the spin system in the phase diagram of Fig. 2 [16].

(i) Disordered folded phase: we do not allow for any spontaneous symmetry breaking in the system. Using rotational symmetry and the symmetry under reversal of all spins, we end up with only four independent weights $Z_{0,1,2,3}$ corresponding to vertices with, respectively, zero, two, four, or six surrounding folds.

(ii) Ferromagnetic phase: we allow for a spontaneous ferromagnetic symmetry breaking ($M\neq 0$). Then the two vertices with no fold have different weight Z_0 and $\overline{Z_0}$ according to their ± 6 magnetization. The other vertices are neutral in this respect and we end up with five different weights.

(iii) Antiferromagnetic phase: we allow for a spontaneous antiferromagnetic symmetry breaking ($M_{\rm st}\neq 0$). Then all weights Z_i have to be doubled into $(Z_i,\overline{Z_i})$ except for the vertex with no fold ($i=0$) which is neutral in the staggered magnetization. We end up with seven different weights.

The spin configurations, their degeneracies, and the notations for their weights are summarized in Table I. Of course, case (i) can be recovered from either case (ii) or (iii) as a particular realization with no spontaneous symmetry breaking (i.e., $Z_i=\overline{Z_i}$ for all i). Also, we assume that the two (ferromagnetic and antiferromagnetic) symmetries cannot be broken simultaneously. We thus need to study only cases (ii) and (iii) above to get the complete phase diagram of the system (here at $h=0$).

At first we consider the ferromagnetic case (ii). In this case, the stationarity condition reduces to the following nonlinear equations between the weights $Z_0,\overline{Z_0},Z_1,Z_2,Z_3$:

$$Z_0=\exp(-\lambda+3K)(y_{++})^3/(y_+)^2,$$

$$\overline{Z_0}=\exp(-\lambda+3K)(y_{--})^3/(y_-)^2,$$

TABLE I. Independent hexagon spin configurations. The corresponding elements of ρ_6 and the degeneracies are indicated.

Spin Conf.	(i) Dis.	(ii) Ferromagnetic	(iii) Antiferromagnetic	Deg.
$++++++$	Z_0	Z_0	Z_0	1
$------$	Z_0	$\overline{Z_0}$	Z_0	1
$++{+}{-}{-}{-}$	Z_1	Z_1	Z_1	3
$---{+}{+}{+}$	Z_1	Z_1	$\overline{Z_1}$	3
$+{-}{-}{+}{+}{-}$	Z_2	Z_2	Z_2	6
$-{+}{+}{-}{-}{+}$	Z_2	Z_2	$\overline{Z_2}$	6
$+{-}{+}{-}{+}{-}$	Z_3	Z_3	Z_3	1
$-{+}{-}{+}{-}{+}$	Z_3	Z_3	$\overline{Z_3}$	1

$$Z_1=\exp(-\lambda+K)(y_{++})(y_{--})(y_{+-})/(y_+)(y_-),$$

$$Z_2=\exp(-\lambda-K)(y_{++})^{1/2}(y_{--})^{1/2}(y_{+-})^2/(y_+)(y_-),$$

$$Z_3=\exp(-\lambda-3K)(y_{+-})^3/(y_+)(y_-), \qquad (3.16)$$

involving a single Lagrange multiplier λ. Here, y_{++}, y_{+-}, y_{--}, y_+, and y_- are two- and one-point functions $\rho_2(\sigma_1\sigma_2)$ and $\rho_1(\sigma_1)$ (there is no difference here between sublattices A and B), which are defined as follows:

$$y_{++}=\rho_2(++)=Z_0+2Z_1+2Z_2,$$

$$y_{+-}=\rho_2(+-)=\rho_2(-+)=Z_1+4Z_2+Z_3,$$

$$y_{--}=\rho_2(--)=\overline{Z_0}+2Z_1+2Z_2,$$

$$y_+=\rho_1(+)=Z_0+3Z_1+6Z_2+Z_3,$$

$$y_-=\rho_1(-)=\overline{Z_0}+3Z_1+6Z_2+Z_3. \qquad (3.17)$$

The above equations imply the following simple relations:

$$\frac{(Z_0\overline{Z_0})^{1/2}}{Z_1}=\frac{Z_1}{Z_2}=\frac{Z_2}{Z_3}=\exp(2K)\,\frac{(y_{++})^{1/2}(y_{--})^{1/2}}{y_{+-}}. \qquad (3.18)$$

Introducing the two reduced variables

$$x\equiv\frac{Z_1}{(Z_0\overline{Z_0})^{1/2}},\quad y\equiv\frac{\overline{Z_0}}{Z_0}, \qquad (3.19)$$

we can express all the weights in terms of x, y, and the normalization factor $w_0\equiv(Z_0\overline{Z_0})^{1/2}$:

$$Z_0=y^{+1/2}w_0,\quad \overline{Z_0}=y^{-1/2}w_0,$$

$$Z_1=xw_0,\quad Z_2=x^2w_0,\quad Z_3=x^3w_0. \qquad (3.20)$$

The above equations (3.16) reduce to the following nonlinear equations for the reduced variables:

$$y=\left(\frac{y+2y^{1/2}(x+x^2)}{1+2y^{1/2}(x+x^2)}\right)^3\left(\frac{1+y^{1/2}(3x+6x^2+x^3)}{y+y^{1/2}(3x+6x^2+x^3)}\right)^2, \qquad (3.21)$$

$$x=\frac{y(x+4x^2+x^3)}{u[1+2y^{1/2}(x+x^2)]^{1/2}[y+2y^{1/2}(x+x^2)]^{1/2}}, \tag{3.22}$$

where $u=\exp(2K)$. The parameter y measures the spontaneous ferromagnetic symmetry breaking while the parameter x measures the fugacity per folded bond.

We can easily see that Eq. (3.21) has two obvious solutions: a solution $y=1$ and x arbitrary and a solution $x=0$ and y arbitrary. The latter solution is also a solution of Eq. (3.22). It means that each vertex of the membrane can be only in one of the two configurations without fold Z_0 or $\overline{Z_0}$. The solution cannot determine the ratio $y=Z_0/Z_0$, i.e., the proportion of each state. However, with only these two vertices at hand, no fold can ever be created and the only possible global states for the lattice are the state with all spins up ($M=1$) and that with all spins down ($M=-1$). The above solution simply describes an arbitrary superposition of these two (symmetric) pure flat states. The fact that the membrane is indeed frozen in a pure completely flat state is further confirmed by computing the entropy that is found to be exactly zero, and by computing the free energy, that is found to be $f=-3K$ per hexagon, as expected (there are three bonds per hexagon).

The first solution with $y=1$ means that the spontaneous symmetry breaking does not occur and that the membrane is in the disordered folded state ($Z_0=\overline{Z_0}$). The value of x is then fixed by Eq. (3.22) [16]:

$$x=\frac{(2-u)+\sqrt{(3-u-u^2)}}{(2u-1)}, \tag{3.23}$$

which has a solution for $K\leqslant\ln[(1+\sqrt{13})/2]/2$. Comparing the corresponding free energy to that of the pure flat state, we get a first-order transition from disordered folded to purely flat at $K_c\sim0.1013$ [16].

We also looked numerically for another nontrivial solution with spontaneous symmetry breaking ($y\neq1$) and intermediate magnetization ($x\neq0$) but did not find any. We conclude that there is no possible flat phase with $0<|M|<1$ and the above three phases ($M=\pm1$ or 0) are the only stable ones for positive K.

As has been discussed previously, the above analysis is also instrumental for the estimation of the probability distribution $\rho_{\tau,6}(\{\tau_i\})$ of the disorder variables τ. We can use indeed for $\rho_{\tau,6}$ the distribution ρ_6 above at $K=h=0$, characterized by $y=1$ and $x=2$ [16]. In other words, if we define $P_{0,1,2,3}$ as the weights $\rho_{\tau,6}$ for the local realizations of disorder with zero, two, four, or six creases around the vertex, we learn that the ratios P_1/P_0, P_2/P_1, and P_3/P_2 must all be identical and equal to two (see Fig. 4). Their values are then fixed by the normalization:

$$2P_0+6P_1+12P_2+2P_3=1 \tag{3.24}$$

leading to [16]

$$P_0=\tfrac{1}{78},\quad P_1=\tfrac{2}{78},\quad P_2=\tfrac{4}{78},\quad P_3=\tfrac{8}{78}. \tag{3.25}$$

More generally, we can parametrize the distribution of P with one parameter α equal to the ratios $\alpha=P_1/P_0=P_2/P_1=P_3/P_2$. Beside the natural value $\alpha=2$ above, the limiting case $\alpha=0$ describes a membrane with no crease and $K_{ij}=K$ everywhere, while $\alpha=\infty$ describes a membrane with creases everywhere and $K_{ij}=-K$ on each bond.

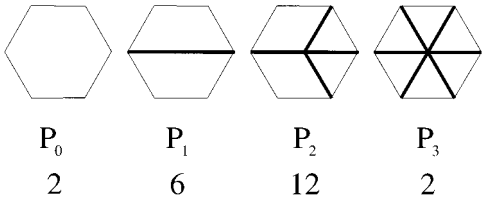

FIG. 4. Probability distribution for each disorder configuration. We also show their degeneracies

Now we discuss the compactly ordered (antiferromagnetic) folded phase (iii). There are seven independent weights for $h=0$ (see Table I) and in this case it is convenient to use staggered variables $\eta_i=(-1)^{i-1}\sigma_i$ with $(-1)^{i-1}=1$ on triangles belonging to the sublattice A and $(-1)^{i-1}=-1$ on triangles belonging to the sublattice B. The corresponding two-point function is simply

$$\rho_{\eta,2}(\eta_1,\eta_2)=\rho_2(\eta_1,-\eta_2). \tag{3.26}$$

About the one-point function, we have the symmetry $\rho_{1A}(\sigma)=\rho_{1B}(-\sigma)$ in the antiferromagnetic phase, leading to only one (A or B independent) one-point function for η:

$$\rho_{\eta,1}(\eta)=\rho_{1A}(\eta)=\rho_{1B}(-\eta). \tag{3.27}$$

As before, the solution of the nonlinear stationarity equations for the seven weights can be parametrized as

$$\begin{gathered}Z_0=w_0,\quad Z_1=xy^{1/2}w_0,\quad \overline{Z_1}=xy^{-1/2}w_0,\\ Z_2=x^2y^{1/2}w_0,\quad \overline{Z_2}=x^2y^{-1/2}w_0,\quad Z_3=x^3y^{3/2}w_0,\\ \overline{Z_3}=x^3y^{-3/2}w_0,\end{gathered} \tag{3.28}$$

with two reduced variables x and y solutions of

$$y=\frac{y_{++}}{y_{--}}\left(\frac{y_-}{y_+}\right)^{2/3},\quad x=u^{-1}\frac{y_{++}^{1/2}y_{--}^{1/2}}{y_{+-}}, \tag{3.29}$$

where

$$\begin{gathered}y_{++}=\rho_{\eta,2}(++)=Z_1+3Z_2+\overline{Z_2}+Z_3,\\ y_{+-}=\rho_{\eta,2}(+-)=\rho_{\eta_2}(-+)=Z_0+Z_1+\overline{Z_1}+Z_2+\overline{Z_2},\\ y_{--}=\rho_{\eta,2}(--)=\overline{Z_1}+3\overline{Z_2}+Z_2+\overline{Z_3},\\ y_+=\rho_{\eta,1}(+)=Z_0+2Z_1+\overline{Z_1}+4Z_2+2\overline{Z_2}+Z_3,\\ y_-=\rho_{\eta,1}(-)=Z_0+2\overline{Z_1}+Z_1+4\overline{Z_2}+2Z_2+\overline{Z_3}.\end{gathered} \tag{3.30}$$

In Eqs. 3.29, the global normalization w_0 drops out, so the equations can be solved for x and y as functions of $u=\exp(2K)$. Again the variable x measures the fugacity for each fold and y measures the antiferromagnetic spontaneous symmetry breaking. Solving the above equations numerically

by iteration, we find a continuous transition from a disordered folded state ($y=1$) to a compactly folded ordered phase ($y\neq 1$) at $K_{\rm st}=-0.2838$. The value of $K_{\rm st}$ can be found simply by linearizing Eqs. 3.29 by writing $y=1+\epsilon$. This fixes the value of x to be the real solution $x_{\rm st}$ of

$$x^3-21x^2-12x-4=0, \tag{3.31}$$

that is

$$x_{\rm st}=7+(387+2\sqrt{223})^{1/3}+53/(387+2\sqrt{223})^{1/3} \tag{3.32}$$

and u to be

$$u_{\rm st}=\frac{1+4x_{\rm st}+x_{\rm st}^2}{1+2x_{\rm st}+2x_{\rm st}^2}. \tag{3.33}$$

IV. RESULTS FOR THE FULLY DISORDERED SYSTEM

In this section we analyze the fully disordered case [Eq. (2.9)] within the CVM approximation. In Sec. IV A, we study the system for $h=0$ for several values of the parameter α for the disorder weights. Next we fix $\alpha=2$ and proceed to the general (K,h) case in Sec. IV B. We obtain the (K,h)-phase diagram by use of the natural iteration method.

A. Analysis with reduced elements of ρ_6 ($h=0$ case)

As in Sec. III, we will study the fully disordered system for $h=0$ by reducing the number of elements of the six-point density matrix. In the case with disorder, the symmetries of the elements of the six-point function $\rho_6(\{\sigma_i\},\{\tau_i\})$ depend also on the symmetry of the disorder (τ variables), in addition to the symmetries of the spin variable $\{\sigma\}$ itself.

In Sec. III B, we have studied the pure model with an antiferromagnetic spontaneous symmetry breaking for $K<0$. There we have used the staggered variables as $\eta_i=(-1)^{i-1}\sigma_i$. If we regard the pure system for $K<0$ as a trivial disordered system with $\rho_{\tau 6}(1,-1,1,-1,1,-1)=1$, i.e., τ_i is fixed to $(-1)^{i-1}$, and $K>0$, the above staggered variables can be written as

$$\eta_i=\sigma_i\tau_i. \tag{4.1}$$

The motivation for introducing the staggered variables is that in these variables the antiferromagnetic order parameter $M_{\rm st}$ is simply written as

$$M_{\rm st}=\frac{1}{N_t}\left\langle\left(\sum_i \eta_i\right)\right\rangle, \tag{4.2}$$

and we do not have to differentiate between the A and B sublattices. That is, the staggered variables $\{\eta_i\}$ are more natural than the original variables $\{\sigma_i\}$ when one discusses the antiferromagnetic symmetric case.

In the fully disordered system, we are mainly interested in the spontaneous symmetry breaking at $K>0$ of the following ''frozen'' order parameter

$$F=\frac{1}{N_t}\overline{\left\langle\left(\sum_i \sigma_i\tau_i\right)\right\rangle}. \tag{4.3}$$

[The reader might wonder whether the $\tau\to-\tau$ symmetry could lead to a zero quenched average of the order parameter. However, this symmetry implies only that whenever $\rho_{\rm min}(\{\sigma\},\{\tau\})$ is a solution of the variational equations, $\rho_{\rm min}(\{\sigma\},\{-\tau\})$ is also a solution, but does not imply that $\rho_{\rm min}(\{\sigma\},\{\tau\})=\rho_{\rm min}(\{\sigma\},\{-\tau\})$.] This order parameter judges whether or not the membrane is trapped in the randomly oriented phase, characterized by the disorder variables $\{\tau_i\}$. As in the antiferromagnetic case, it is natural to use the following ''gauged'' variables:

$$\eta_i=\sigma_i\tau_i. \tag{4.4}$$

Using these new gauged variables, we classify the elements of six-point functions by the symmetries of both the spin configuration and the disorder configuration. Hereafter we only consider the system for $h=0$ and allow for two types of solutions that correspond to whether the frozen order exists ($F\neq 0$) or not ($F=0$).

(i) Disordered folded phase: we do not allow for any spontaneous symmetry breaking in the system (M, $M_{\rm st}$, and $F=0$). Each of the four elementary types of disorder configuration (with zero, two, four or six creases) leaves us with a certain number of symmetries, including that under reversal of all spins. We use these symmetries on the η variables to reduce the number of weights. We end up with only 22 independent weights in this case.

(ii) Frozen phase: we allow for a spontaneous symmetry breaking of the frozen order parameter ($F\neq 0$). Then all weights have to be doubled except for those vertices that are neutral in the gauged magnetization ($\Sigma_1^6\eta_i=0$). We end up with 38 different weights in this case.

In Fig. 5, we have summarized the results of this symmetry analysis in case (ii). Note that case (i) can always be seen as a particular case of case (ii) with extra symmetries. On the left-hand side of each group, we show the disorder configuration $\{\tau_i\}$. To its right, we present the spin configurations $\{\eta_i\}$ that are independent from each other. We also indicate the notations for their weights and their degeneracies. The two indices i,j in $Z_{i,j}$ indicate a configuration with $2i$ creases and $2j$ folds in the σ variable.

In terms of these elements of the six-point function, we define the two-point functions as follows:

$$\begin{aligned}
y_{0,0}^{\pm}&=Z_{0,0}^{\pm}+2Z_{0,1}+2Z_{0,2}+2Z_{1,0}+2Z_{1,1}^{\pm}+2\widetilde{Z}_{1,1}^{\pm}+2Z_{1,2}^{\pm}\\
&\quad+2\widetilde{Z}_{1,2}^{\pm}+2Z_{2,0}+2Z_{2,1}^{\pm}+2\widetilde{Z}_{2,1}^{\pm}+2Z_{2,2}^{\pm}+2\hat{Z}_{2,2}^{\pm},\\
y_{0,1}&=Z_{0,1}+4Z_{0,2}+Z_{0,3}+\widetilde{Z}_{1,1}^{+}+\widetilde{Z}_{1,1}^{-}+Z_{1,2}^{+}+Z_{1,2}^{-}+3\widetilde{Z}_{1,2}^{+}\\
&\quad+3\widetilde{Z}_{1,2}^{-}+Z_{1,3}^{+}+Z_{1,3}^{-}+\widetilde{Z}_{2,1}^{+}+\widetilde{Z}_{2,1}^{-}+\overline{Z_{2,2}^{+}}+\overline{Z_{2,2}^{-}}+2\widetilde{Z}_{2,2}^{+}\\
&\quad+2\widetilde{Z}_{2,2}^{+}+\hat{Z}_{2,2}^{+}+\hat{Z}_{2,2}^{-}+Z_{2,3}^{+}+Z_{2,3}^{-},\\
y_{1,0}&=y_{0,1}(Z_{i,j}\to Z_{j,i}),\\
y_{1,1}^{\pm}&=Z_{1,1}^{\pm}+Z_{1,2}^{\pm}+Z_{1,2}^{\mp}+2\widetilde{Z}_{1,2}^{\pm}+Z_{1,3}^{\pm}+Z_{2,1}^{\pm}+Z_{2,1}^{\mp}+4Z_{2,2}^{\pm}\\
&\quad+2\overline{Z_{2,2}^{\pm}}+4\hat{Z}_{2,2}^{\pm}+2\hat{Z}_{2,2}^{\mp}+4\widetilde{Z}_{2,2}^{\pm}+3Z_{2,3}^{\pm}+Z_{2,3}^{\mp}+2\widetilde{Z}_{2,1}^{\pm}\\
&\quad+Z_{3,3}^{\pm}+3Z_{3,2}^{\pm}+Z_{3,2}^{\mp}+Z_{3,1}^{\pm}.
\end{aligned} \tag{4.5}$$

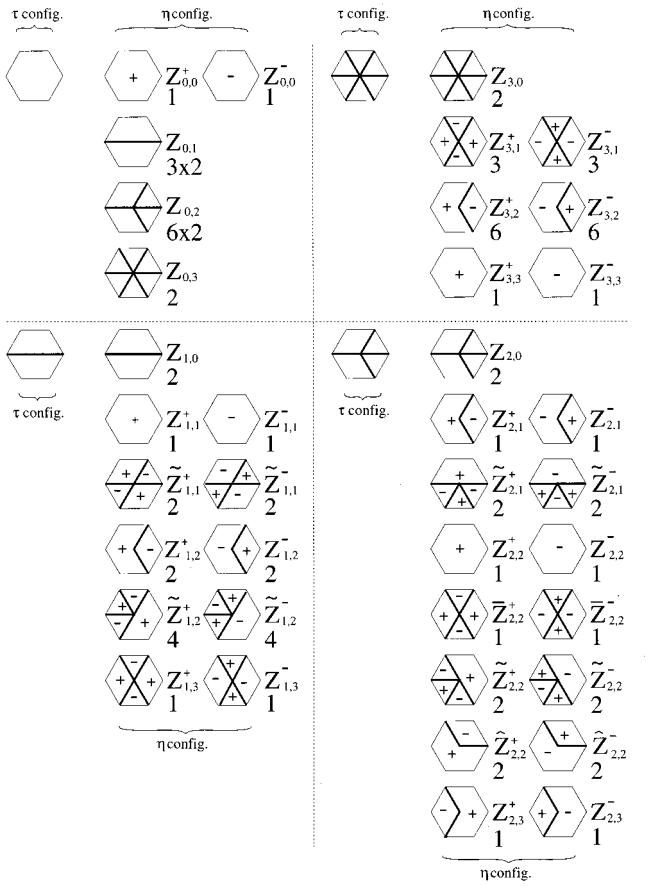

FIG. 5. The 38 independent local fold environments for each vertex for the four different local realizations of disorder (zero, two, four, or six creases). Each disorder configuration is shown at the left-hand side of each group. To their right, we show the spin configurations, the weights, and the degeneracies. We have represented by thick lines the domain walls for the gauged spin variable $\eta_i=\sigma_i\tau_i$. A subscript i,j indicates a configuration with $2i$ creases and $2j$ folds. The superscript $\pm$ indicates a $\pm$ contribution to F. In a $F=0$ phase, equating the $+$ and $-$ weights leaves us with 22 independent weights.

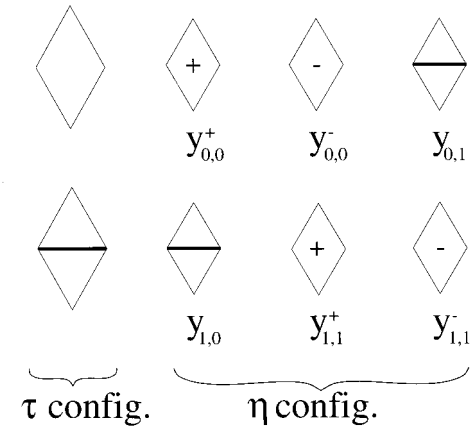

FIG. 6. Definitions of two-point functions. Gauged spin variables $\eta_i=\sigma_i\tau_i$ are used. On the left-hand side, we show the disorder configuration τ.

The superscript of y means that the gauged spin configuration $\{\eta_i\}$ have the corresponding positive (or negative) contribution to F (see Fig. 6). Again, the first subscript indicates whether there is a crease line (1) or not (0). The second subscript means that there is a fold (1) or not (0) in the original σ variables. Based on these two-point functions, we also introduce the following one-point functions:

$$y^{\pm}=y^{\pm}_{0,0}+y_{0,1}+y_{1,0}+y^{\pm}_{1,1}. \tag{4.6}$$

In terms of these functions, we write down the stationarity conditions. For example, let us show those for $Z^{\pm}_{0,0}$, $Z_{0,1}$, $Z_{0,2}$, and $Z_{0,3}$:

$$Z^{+}_{0,0}=\exp(-\lambda_0+3K)(y^{+}_{0,0})^3/(y^{+})^2,$$

$$Z^{-}_{0,0}=\exp(-\lambda_0+3K)(y^{-}_{0,0})^3/(y^{-})^2,$$

$$Z_{0,1}=\exp(-\lambda_0+K)(y^{+}_{0,0})(y^{-}_{0,0})(y_{0,1})/(y^{+})(y^{-}),$$

$$Z_{0,2}=\exp(-\lambda_0-K)(y^{+}_{0,0})^{1/2}(y^{-}_{0,0})^{1/2}(y_{0,1})^2/(y^{+})(y^{-}),$$

$$Z_{0,3}=\exp(-\lambda_0-3K)(y_{0,1})^3/(y^{+})(y^{-}). \tag{4.7}$$

Here, due to the above symmetries, we need only four Lagrange multipliers $\lambda_{0,1,2,3}$, one for each of the four elementary types of disorder in Fig. 4. These Lagrange multipliers are of course determined by the normalization conditions, like

$$Z^{+}_{0,0}+Z^{-}_{0,0}+6Z_{0,1}+12Z_{0,2}+2Z_{0,3}=P_0. \tag{4.8}$$

As in the pure case, we introduce reduced variables. Here we need four ratios x, y, s, and t defined as

$$x=u^{-1}\frac{y_{0,1}}{(y^{+}_{0,0}y^{-}_{0,0})^{1/2}},\quad y=u^{-1}\frac{y_{1,0}}{(y^{+}_{1,1}y^{-}_{1,1})^{1/2}},$$

$$s=\left(\frac{y^{+}_{0,0}}{y^{-}_{0,0}}\right)^{1/2}\left(\frac{y_{-}}{y_{+}}\right)^{1/3},\quad t=\left(\frac{y^{+}_{1,1}}{y^{-}_{1,1}}\right)^{1/2}\left(\frac{y_{-}}{y_{+}}\right)^{1/3}, \tag{4.9}$$

and for convenience, we also introduce the following averaged weights:

$$w_0=(Z^{+}_{0,0}Z^{-}_{0,0})^{1/2},\quad w_1=(Z^{+}_{1,1}Z^{-}_{1,1})^{1/2},$$

$$w_2=(Z^{+}_{2,2}Z^{-}_{2,2})^{1/2},\quad w_3=(Z^{+}_{3,3}Z^{-}_{3,3})^{1/2}. \tag{4.10}$$

The stationarity conditions are then reduced to the following simple form:

$$Z^{\pm}_{0,0}=s^{\pm 3}w_0,\quad Z_{0,1}=xw_0,\quad Z_{0,2}=x^2w_0,\quad Z_{0,3}=x^3w_0,$$
$$Z_{3,0}=y^3w_3,\quad Z^{\pm}_{3,1}=y^2t^{\pm 1}w_3,\quad Z^{\pm}_{3,2}=yt^{\pm 1}w_3,$$
$$Z^{\pm}_{3,3}=t^{\pm 3}w_3,\quad Z_{1,0}=yw_1,\quad Z^{\pm}_{1,1}=s^2t^{\pm 1}w_1,$$
$$\widetilde{Z}^{\pm}_{1,1}=xys^{\pm 1}w_1,\quad Z^{\pm}_{1,2}=xs^{\pm 1}w_1,$$
$$\widetilde{Z}^{\pm}_{1,2}=x^{3/2}y^{1/2}(st)^{\pm 1/2}w_1,\quad Z^{\pm}_{1,3}=x^2t^{\pm 1}w_1,$$
$$Z_{2,0}=y^2w_2,\quad Z^{\pm}_{2,1}=ys^{\pm 1}w_2,$$
$$\widetilde{Z}^{\pm}_{2,1}=x^{1/2}y^{3/2}(st)^{\pm 1/2}w_2,\quad Z^{\pm}_{2,2}=s^{\pm 1}t^{\pm 2}w_2,$$
$$\overline{Z^{\pm}_{2,2}}=xyt^{\pm 1}w_2,\quad \widetilde{Z}^{\pm}_{2,2}=xyt^{\pm 1}w_2,$$
$$\hat{Z}^{\pm}_{2,2}=x^{1/2}y^{1/2}(st)^{\pm 1/2}w_2,\quad Z^{\pm}_{2,3}=xt^{\pm 1}w_2. \qquad (4.11)$$

Each weight $Z_{i,j}$ is given as the product of w_i by a simple function of x, y, s, and t. The rules for the x and y variables are simple: The disorder configuration splits the bonds into those that support a crease and those that do not. On the bonds with no crease, we assign a factor $\sqrt{x}$ if the bond has a fold and 1 otherwise. On the bonds with a crease, we assign a factor $\sqrt{y}$ if the bond has no fold and 1 otherwise. In both cases, the nontrivial factor is assigned if the gauged variable changes sign when crossing the bond. About the factors of s and t, the rules are more subtle. Still s and t both measure the symmetry breaking of the frozen parameter.

The weights $w_{0,1,2,3}$ can be expressed as functions of x, y, s, and t thanks to the normalization conditions as follows:

$$P_0=w_0[s^3+s^{-3}+6x+12x^2+2x^3],$$
$$P_1=w_1[2y+s^2t+s^{-2}t+2xyz+2xyz^{-1}+2xy+2xy^{-1}+4x^{3/2}y^{1/2}s^{1/2}t^{1/2}+4x^{3/2}y^{1/2}s^{-1/2}t^{-1/2}+x^2t+x^2t^{-1}],$$
$$P_2=w_2[2y^2+ys+ys^{-1}+2x^{1/2}y^{3/2}s^{1/2}t^{1/2}+2x^{1/2}y^{3/2}s^{-1/2}t^{-1/2}+st^2+s^{-1}t^{-2}+3xyt+3xyt^{-1}+2x^{1/2}y^{1/2}s^{1/2}t^{1/2}+2x^{1/2}y^{1/2}s^{-1/2}t^{-1/2}+xt+xt^{-1}],$$
$$P_3=w_3[t^3+t^{-3}+6y(t+t^{-1})+3y^2(t+t^{-1})+2y^3]. \qquad (4.12)$$

In Eq. (4.9), the right-hand side of each equation is thus a function of x, y, s, and t only. These equations can be simply solved numerically by iteration.

Hereafter we show the results of this numerical analysis. We first fix $\alpha=2$ for the weights $P_{0,1,2,3}$. We start the iteration for $K=0$ with a fully symmetric solution that corresponds to a disordered phase. We proceed to the iteration until the required precision is reached. We then increase K by dK and restart the iteration. For this next value of K, we start the iteration from the solution of the iteration for the previous value of K. This procedure allows us to follow the continuous evolution with K of a given local minimum of the free energy. We increase K from 0 to 0.2 and then decrease it back to 0. In this way, if the system has a first-order transition with two local minima of the free energy in competition, the method will show a hysteresis. Note that this iteration procedure is slightly different from the natural iteration method that we shall use in Sec. IV B, where we search a solution for the nonlinear stationarity equations from different initial assumptions corresponding to the different possible symmetries.

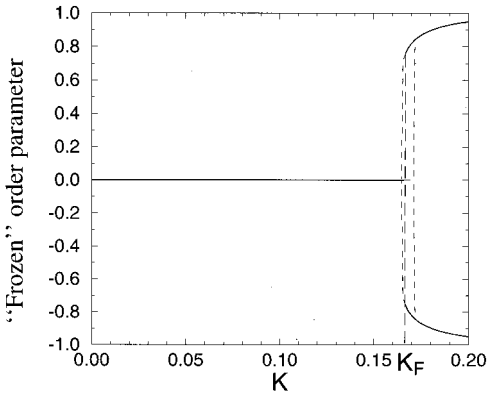

FIG. 7. Frozen order parameter F versus bending rigidity K. F changes from $F=0$ to $F\neq 0$. The system shows a hysteresis with two separate jumps for two values of K on each side of K_F. The position of K_F is determined precisely by comparing the free energies of both phases, as shown in the next figure.

In Fig. 7, we show the behavior of the frozen order parameter F as a function of the bending rigidity K. For small K ($<K_F$), F is clearly zero and the system is in a disordered folded phase. At K_F, the system shows a first-order transition from this disordered folded phase to a frozen phase $F\neq 0$. The value of $|F|$ is strictly less than 1, thus the system is only partially frozen. When the iteration is performed with first increasing K and then decreasing it back to zero, we see a clear hysteresis with two jumps on both sides of K_F. The value of the transition point K_F can be fixed precisely by comparing the value of the free energies for both phases. This is shown in Fig. 8. The hysteresis allows us to see clearly the crossing of the two free-energy lines correspond-

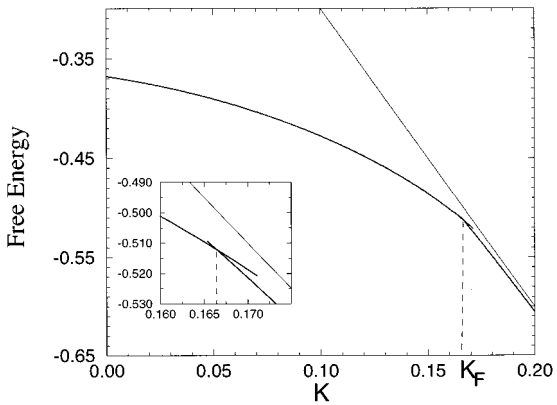

FIG. 8. Free energy f per hexagon versus bending rigidity K. The thin straight line corresponds to a completely frozen phase $F=1$. This phase is never stable. The two thick lines correspond to disordered folded phase $F=0$ (for small K) and to the frozen phase $0<|F|<1$ (for larger K). The two lines cross at the transition point K_F. As shown in the inset, we find $K_F\sim 0.166(1)$.

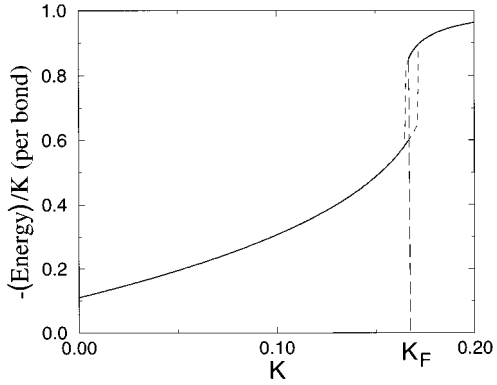

FIG. 9. Gauged two-point function $\overline{\langle \eta_1 \eta_2 \rangle} = -(\text{internal energy})/K$ versus K. We see here also a clear evidence of first-order transition with a hysteresis.

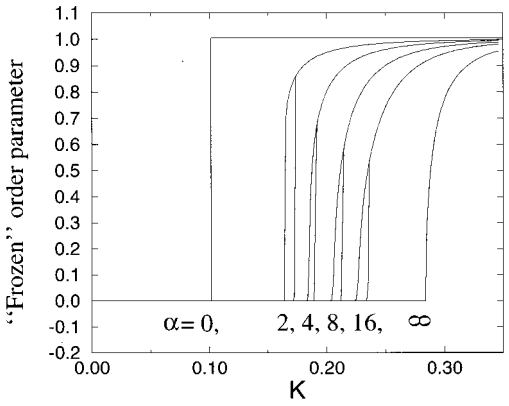

FIG. 10. Frozen order parameter F versus K for several values of α (we only show here the case $F \geqslant 0$). The jump in the order parameter becomes smaller as α becomes larger. The continuous character of the transition is recovered at $\alpha = \infty$ (pure antiferromagnetic system). For intermediate α, the iteration gives rise to a hysteresis.

ing to both phases $F=0$ and $F \neq 0$. Indeed the system stays for some time after the transition point in the wrong metastable state. As shown in the inset of the figure, the transition occurs at $K_F \sim 0.166(1)$.

Figure 9 shows the behavior of the two-point function $\overline{\langle \eta_1 \eta_2 \rangle} = -(\text{internal energy})/K$ versus K. It also shows clear evidence of first-order transition with a hysteresis in the results of the iteration procedure. At $K=0$, the disorder variables τ_i and spin variables σ_i decouple. The value of the function is then $\overline{\langle \eta_1 \eta_2 \rangle} = \overline{\tau_1 \tau_2} \langle \sigma_1 \sigma_2 \rangle_{\text{at } K=0} = (-\frac{1}{3}) \times (-\frac{1}{3}) = \frac{1}{9}$, as found here (the value $-\frac{1}{3}$ is easily obtained from the analysis of the pure case at $K=0$ of Sec. III B [16]).

Next, we studied the system for several values of the parameter α for the disorder weights. As has been explained previously, $\alpha=0$ means that there is no crease in the system and $\alpha=\infty$ corresponds to the pure antiferromagnetic system. From the previous analysis, we know that the system shows a first-order transition for both $\alpha=0$ and $\alpha=2$ above. At $\alpha=0$ (where $F=M$) the transition is from $F=M=0$ to $F=M=\pm 1$ [15]. At $\alpha=2$, the discontinuity is smaller with $|F|<1$ in the frozen phase. We also know that the transition becomes continuous and second order at $\alpha=\infty$ [16]. The transition point is at $K=0.284$ as obtained before. From the results in Fig. 10, we see that the discontinuity of the transition becomes smaller as we increase the parameter α. The continuity of the transition seems to be recovered only at $\alpha=\infty$, although it is difficult to determine whether the transition is of first order or of second order when the discontinuity becomes too small.

B. (K,h) phase diagram

Let us now turn to the analysis of the whole phase diagram in the (K,h) plane. It is, of course, symmetric with respect to the $h=0$ axis. It is shown in Fig. 11 for $h \geqslant 0$ as obtained from the CVM stationarity equations solved by the natural iteration method [21]. Here we have set $\alpha=2$ again and the results were obtained with a set of 22×22 independent weights, i.e., without making any assumption on the symmetries of the different phases, except in the initial conditions of the iteration. At sufficiently large values of h and for $h>2K$, the completely flat phase with $M=1$ is stable with respect to both the disorder and the thermal fluctuations. At sufficiently large values of K and for $h<2K$, the system is in a frozen phase with $M=0$, $M_{\text{st}}=0$, and $F \sim 1$. There is a first-order transition line between these two phases, which is roughly given by $h=2K$. The position of the line can be obtained by requiring that the free energy of the completely flat phase and that of the frozen phase take the same value, i.e., by solving the equation $f_{\text{c.flat}} = f_{\text{frozen}}$. About $f_{\text{c.flat}}$, the bending energy contribution per hexagon is estimated as $-3K\overline{\langle \tau_1 \tau_2 \sigma_1 \sigma_2 \rangle} = -3K(\overline{\tau_1 \tau_2}) = -3K \times (-\frac{1}{3}) = K$, while the entropy vanishes in the absence of local excitations. We thus get the exact free energy $f_{\text{c.flat}} = -2h + K$. The estimation of f_{frozen} is more difficult and we simply assume that $f_{\text{frozen}} \simeq -3K$ as in a completely frozen phase, because the frozen order parameter F is almost saturated to 1. From these estimations, we obtain the transition line $h \simeq 2K$, which is what we indeed observe.

For smaller K and h, the system is in a disordered folded phase with $F=0$ and $M \sim 0$. As for the pure system, M does not vanish exactly for $h>0$ but still remains very small. This

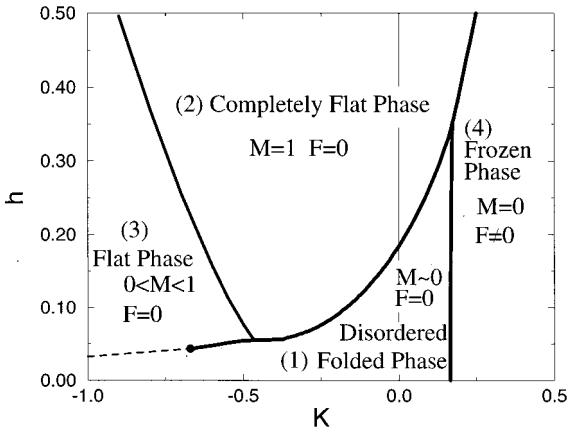

FIG. 11. Phase diagram in the (K,h) plane for the fully disordered system [Eq. (2.9)]. First-order lines separate the four phases: (1) Disordered folded phase with $M \sim 0$, $F=0$, (2) completely flat phase with $M=1$ and $F=0$, (3) flat phase with $0<|M|<1$ and $F=0$ and (4) frozen phase with $M=0$ and $|F|>0$.

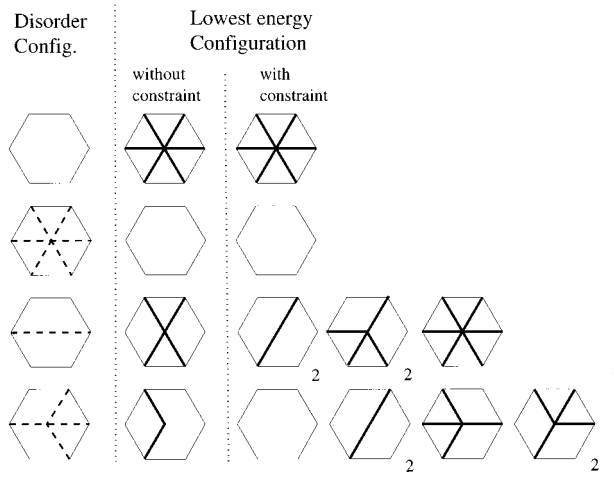

FIG. 12. Lowest-energy spin configurations $\{\sigma_i\}$ for each type of disorder configuration. Folds are indicated by thick lines and creases by dashed lines. On the left-hand side, we show the disorder configurations, in the center the corresponding lowest-energy state, which violates the local folding constraint for the disorders with one and two creases, and on the right-hand side the lowest-energy states that preserve the constraint, together with their degeneracy.

might be an artifact of the CVM approximation [16]. At $K=0$, the spin variables σ are decoupled from the disorder variables τ and the fully disordered system is the same as the pure system. It has a first-order transition point at $h\sim 0.184$ [15]. For $h=0$, the above results confirm those of previous sections with a transition at $K=K_F$.

We have also studied the case of negative K, although it is not very physical. Still, it presents interesting features in view of our further study of other types of disorder in Sec. V. In the usual Mattis model without constraint and for $h=0$, the spins develop at large enough negative K an ''antiferromagneticlike'' order in the gauged variable η_i with a ground state $\eta_i=(-1)^{i-1}$ in the limit $K=-\infty$. Here such order cannot be reached in general due to the constraint on σ, hence on η. If the disorder has zero or three creases, then the ground state $\eta_i=(-1)^{i-1}$ can be reached and is the unique ground-state spin configuration. On the other hand, if it has one or two creases, it cannot be reached and we are led to several lowest-energy spin configurations, as shown in Fig. 12. At $K=-\infty$ and $h=0$, the actual ground state will thus be degenerate with frustrations in the system that might prevent the emergence of a true ''frozen antiferromagnetic'' order. The system is thus always disordered in contrast with the pure case where an antiferromagnetic order had developed.

From the analysis of the lower-energy states, we can easily compute the two-point correlation at $K\to-\infty$, $c=\overline{\langle\sigma_1\tau_1\sigma_2\tau_2\rangle}$ for the gauged variable (i.e., the internal energy/K). For a disorder with zero or three creases, we have $\Sigma_{i \text{ around } v}\langle\sigma_i\tau_i\sigma_{i+1}\tau_{i+1}\rangle=-6$ in the lowest-energy state. For a disorder with one or two creases, we have $\Sigma_{i \text{ around } v}\langle\sigma_i\tau_i\sigma_{i+1}\tau_{i+1}\rangle=-2$ for all the lowest-energy states. The averaged value is thus estimated as $c=\overline{\langle\sigma_1\tau_1\sigma_2\tau_2\rangle}=[-6(P_0+P_3)-2(P_1+P_2)]/6=-19/39\sim-0.48$. This is what we observe (see Fig. 13). The two-point function does not show any discontinuity in all the negative

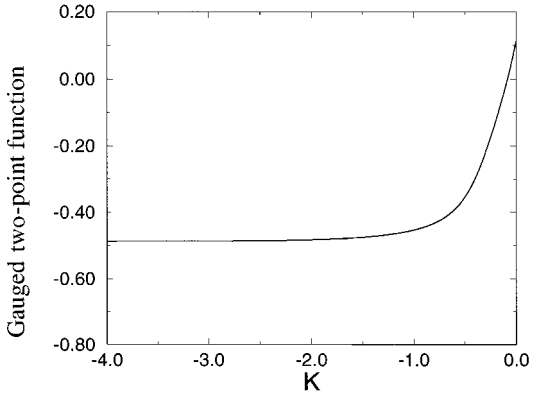

FIG. 13. Gauged two-point function $\overline{\langle\eta_1\eta_2\rangle}=\overline{\langle\sigma_1\tau_1\sigma_2\tau_2\rangle}$ along the K axis ($K<0$, $h=0$).

K regime, which confirms the absence of transition in this regime (at $h=0$).

Finally, we included in Fig. 11 the results of the CVM analysis for negative K and arbitrary h. We can see the emergence of a new partially flat phase with $0<|M|<1$. The nature of the transition between this phase and the disordered folded phase is unclear, in particular because in the latter phase, M is not exactly zero within the CVM approximation. We then see a limiting point (black circle in Fig. 11) below which the magnetization does not present any longer a discontinuity between the two phases. This also might be an artifact of the CVM, in which case the true transition line should be continued to lower values of K (dashed line).

V. OTHER MODELS

In this section, we complete our study by considering other variants of the disorder. As discussed in Sec. II, there are several possibilities for the choice of K_{ij}. In order to appreciate the importance of the local folding constraint (2.1) on the disorder face variables τ_i, we will study the model Hamiltonian (2.9) without the local folding constraint on τ_i. Next we will study the Edwards-Anderson model with the local folding constraint on the spin variables σ_i and a bending term K_{ij} given by $K_{ij}=K\tau_{ij}$ with a random variable $\tau_{ij}=\pm1$ on each bond (ij). We refer to the former case as model (2) and to the latter case as model (3). The difference between models (2) and (3) is simply the possibility in model (3) of having vertices with an odd number of surrounding creases. We also refer to the original model (2.9) with the folding constraint on τ_i as model (1).

Before we discuss the corresponding (K,h) phase diagrams, let us discuss the two-point function of the system at $h=0$ and large K. Clearly in this limit, for a fixed disorder configuration, the σ_i variables will tend to minimize the energy $-K_{ij}\sigma_i\sigma_j$, i.e., will tend to maximize the overlap with the disorder configuration in terms of folded bonds. In other words, the system wants to create a fold ($\sigma_i\sigma_j=-1$) whenever a crease exists ($K_{ij}/K=-1$), and no fold otherwise. For an arbitrary environment of K_{ij} around a vertex, we can easily find one corresponding lowest-energy state for the σ variables around the vertex. There are, in general, several such states. In Fig. 14, we have displayed all disorder environments together with one of the corresponding lowest-energy state. It is interesting to notice that the disorder configura-

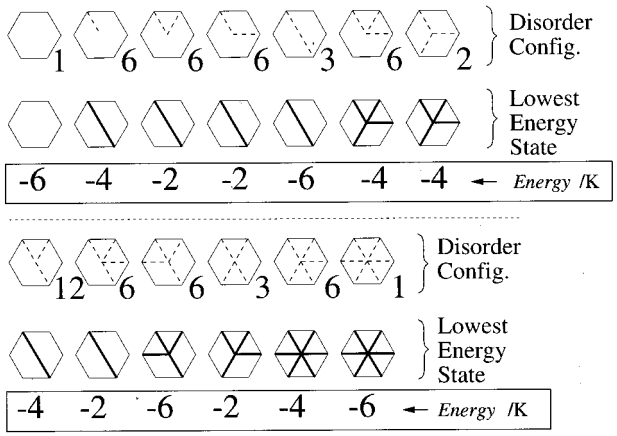

FIG. 14. One of the lowest-energy spin configurations $\{\sigma_i\}$ for each type of disorder configuration. Folds are shown by thick lines and creases by dashed lines. The degeneracies for the disorder configurations are indicated. We also give the value of the corresponding minimal energy.

tions can be arranged in three categories.

(i) Those with an even number of creases and that satisfy the folding constraint. The lowest-energy state is unique and has energy $-6K$.

(ii) Those with an even number of creases but which do not satisfy the folding constraint. The corresponding minimal energy is $-2K$ in this case.

(iii) Those with an odd number of creases. The corresponding minimal energy is $-4K$ in this case.

Of course, in model (2), only vertices of type (i) and (ii) are allowed while in model (3), all vertices can appear.

At $K\to\infty$ and $h=0$, we can thus estimate the two-point function $\overline{\langle\eta_1\eta_2\rangle}=\overline{\langle\sigma_1\tau_1\sigma_2\tau_2\rangle}$ for model (2) and $\overline{\langle\sigma_1\tau_{12}\sigma_2\rangle}$ for model (3) by averaging over all disorder environments the corresponding minimal energy. All (allowed) disorder environments are now equiprobable. Taking into account the appropriate degeneracies under rotations, we get for model (3),

$$\begin{aligned}\overline{\langle\sigma_1\tau_{12}\sigma_2\rangle}=(&-6\times1-6\times1-4\times6-2\times6-2\times6-6\times3\\&-4\times6-4\times2-4\times12-2\times3-2\times6-6\times6\\&-4\times6)/(6\times64)=59/96\sim0.614.\end{aligned}\tag{5.1}$$

For model (2) we find easily

$$\overline{\langle\sigma_1\tau_1\sigma_2\tau_2\rangle}=18/32\sim0.562.\tag{5.2}$$

Note that the above calculation assumes that a lowest-energy state can be constructed globally out of these local lowest-energy configurations. This assumption is acceptable within the CVM approximation at least. We show on Fig. 15 the two-point function for models (2) and (3) as obtained from the CVM. They do not display any discontinuity and tend to the values calculated above at large K. Note also that in some sense, model (3) is less frustrated than model (2) since

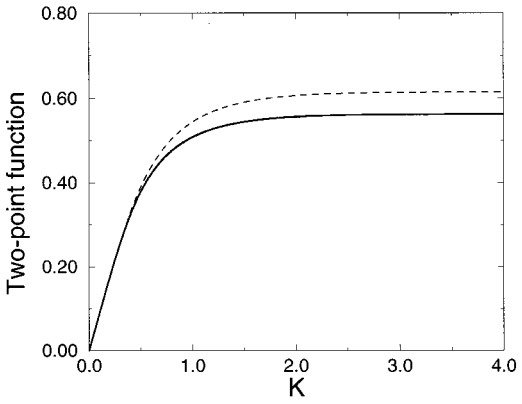

FIG. 15. Gauged two-point function $\overline{\langle\sigma_1\tau_1\sigma_2\tau_2\rangle}$ for model (2) (solid line) and $\langle\sigma_1\tau_{12}\sigma_2\rangle$ for model (3) (dashed line) versus K for $h=0$.

a better overlap with a constrained σ configuration can be obtained for those frustrated disorder environments with an odd number of creases.

We have studied the phase diagrams of both models (2) and (3) within the CVM approximation by use of the natural iteration method [21]. In order to characterize each phase, in addition to the previous order parameters M and F we will also use the spin-glass order parameter q defined in Eq. (2.7), generalized to the case where $M\neq0$:

$$q=\frac{1}{N_t}\sum_i[\overline{\langle\sigma_i\rangle^2}-\overline{(\langle\sigma_i\rangle)^2}].\tag{5.3}$$

In model (2), both F and q measure the frozen character of the phase. They are expected to be zero (nonzero) simultaneously for our choice of disorder distribution. In model (3) with no face τ_i variables, F is not defined any longer and we will use q as a measure of the frozen character of the phase. The phase diagram for the model (2) is shown in Fig. 16 and that for the model (3) in Fig. 17. They are, of course, sym-

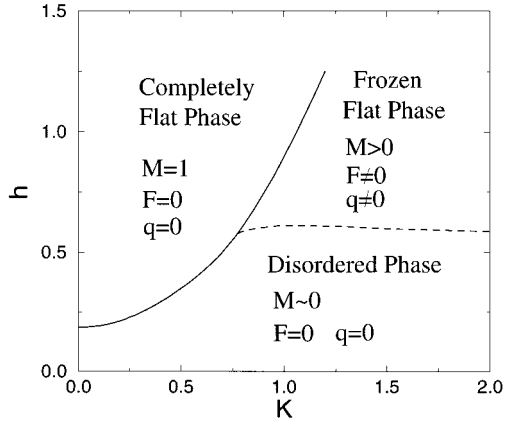

FIG. 16. Phase diagram in the (K,h) plane for model (2). We find three phases: (1) a disordered phase with $F=q=0$, (2) a completely flat phase with $M=1$ and $F=q=0$, and (3) a frozen flat phase with $0<M<1$, $q>0$ and $F>0$. The solid line represents a first-order transition line and the dashed line a continuous transition line.

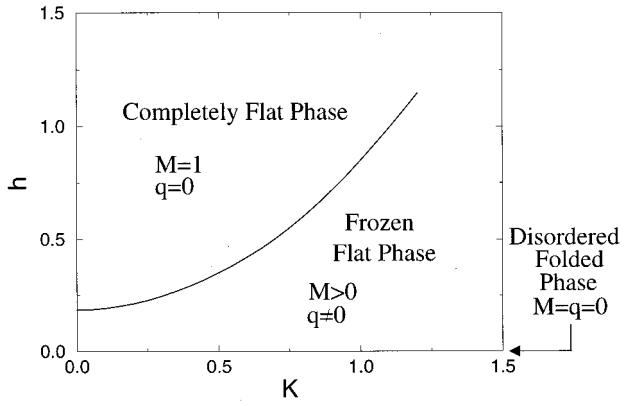

FIG. 17. Phase diagram in the (K,h) plane for model (3). Two phases are separated by a first-order transition line: (1) a frozen flat phase with $0<M<1$ and $q>0$ and (2) a completely flat phase with $M=1$ and $q=0$. The disordered folded phase with $M=q=0$ is recovered only at $h=0$.

metric with respect to the $K=0$ axis but also with respect to the $h=0$ axis. This is because the transformation $\tau_i \to (-1)^{i-1}\tau_i$ in model (2) and $\tau_{ij} \to -\tau_{ij}$ in model (3) exchange equally probable disorder environments and simply change K into $-K$. We only display the phase diagrams for $K>0$ and $h>0$.

At $K=0$, both systems are identical to the pure system and undergo a first-order transition at $h\sim 0.184$ to a completely flat phase. This completely flat phase with $|M|=1$ and $q=0$ is stable for all K at large enough h above a line which is almost the same for the two models up to the tricritical point of Fig. 16. At $h=0$, both systems remain in a disordered folded phase with $M=q=0$ for any value of K. This is different from model (1) where we had a transition to a frozen phase at $K=K_F$. The absence of a frozen phase at $h=0$ is again due to the presence of frustration in the system leading to several competing lowest-energy states.

For fixed (large enough) K and increasing h, models (2) and (3) display different behaviors. As far as q is concerned, model (3) develops a nonzero value of q for any $h>0$. On the other hand, q remains zero in model (2) until a critical value of h is reached where a continuous transition to $q\neq 0$ occurs. For both models, the ''frozen'' phase with $q\neq 0$ also has $0<|M|<1$, and is thus partially flat. As to the $q=0$ phase of model (2), we see a nonzero value of M that is indeed non-negligible close to the continuous transition line. Still we cannot exclude that this could be, again, an artifact of the CVM approximation. Indeed, by continuity from the $K=0$ line, we would rather expect $M=0$ everywhere in this phase. This issue is thus not fully solved. Finally, the absence of the $q=0$ phase in model (3) (except for $h=0$) might also be interpreted again as an indication of a weaker frustration as compared to model (2).

VI. DISCUSSION AND CONCLUDING REMARKS

In this paper we have studied the folding of the triangular lattice in the presence of a quenched random bending rigidity $K_{ij}=\pm K$ and a magnetic field h. We have considered three types of quenched randomness (1) $K_{ij}=K\tau_i\tau_j$ with face random variables $\tau_i=\pm 1$ subject to the folding constraint (2.1); (2) $K_{ij}=K\tau_i\tau_j$ without the folding constraint on the τ_i's; (3) $K_{ij}=K\tau_{ij}$ with a bond random variable $\tau_{ij}=\pm 1$. In case (1), the folding constraint on the disorder variables was introduced to describe a particular type of ''physical'' disorder supposed to mimic that induced in a randomly crumpled surface, here in the context of the folding of the triangular lattice. Applying the cluster variation method generalized to random systems, we have studied the phase diagrams of the three models (1), (2), and (3) and their phase transitions. The phase diagrams for each case are depicted in Figs. 11, 16, and 17, respectively. The most important difference between model (1) and models (2) and (3) is that, in the absence of magnetic field, a frozen phase is found only in model (1), for large enough K. In this phase, the configuration of the triangular lattice is trapped in the randomly oriented phase characterized by the configuration of the disorder variables $\{\tau_i\}$. Models (2) and (3) do not present such frozen order at $h=0$. Indeed, these models, where the quenched randomness is not constrained, have strong frustrations because the constrained spins describing the normals to folded configuration fail to be in the ''virtual'' lowest-energy ground state dictated by the unconstrained disorder, even if the coupling constant K becomes large. For $h>0$, a frozen phase is recovered in models (2) and (3). We find several first-order or continuous transition lines between the frozen phase and a completely flat phase or a disordered folded phase.

At last we make one comment about previous studies on another spin model describing a polymerized membrane with quenched random spontaneous curvature [27,28], with Hamiltonian

$$\mathcal{H}=-\sum_{ij} K\vec{n}_i\cdot\vec{n}_j-\sum_{ij}\vec{D}_{ij}\cdot(\vec{n}_i\times\vec{n}_j). \tag{6.1}$$

Here $\vec{n}$ denotes the normal vector to the membrane embedded in 3D space. The first term is a bending rigidity term and K is the bending rigidity modulus. The second term is a random spontaneous curvature term with a Gaussian probability distribution for $\vec{D}_{ij}$ with variance

$$\langle \vec{D}_{ij}^2\rangle=\Gamma^2. \tag{6.2}$$

In particular, it does not satisfy ''physical'' constraints of a spontaneous curvature that would have been induced by crumpling. Within a mean-field study, it was concluded in [27,28] that the model has a wrinkled phase in the (K,Γ) plane with nonzero spin-glass order parameter $q\neq 0$. This is to be contrasted with our results where the existence of such a phase was crucially requiring the ''physical'' constraint on the disorder variable. However, it is not yet clear whether our conclusions for a quenched random rigidity are applicable to the quenched random spontaneous curvature case. To study the folding of the triangular lattice with random spontaneous curvature, we would need to go to a three-dimensional embedding space. One possibility is to introduce disorder in the 96-vertex model of Ref. [17]. This is left for future study.

ACKNOWLEDGMENTS

One of the authors (S.M.) thanks Dr. Y. Ozeki for suggesting several important references about the cluster varia-

tional method and thanks the JSPS for financial support. We thank Henri Orland for a critical reading of the manuscript.

[1] *Statistical Mechanics of Membranes and Surfaces*, Proceedings of the Fifth Jerusalem Winter School, edited by D. R. Nelson, T. Piran and S. Weinberg (World Scientific, Singapore, 1989).
[2] D. R. Nelson, in *Fluctuating Geometries in Statistical Mechanics and Field Theory*, edited by F. David, P. Ginsparg, and J. Zinn-Justin, Les Houches Session LXII (Elsevier Science, The Netherlands, 1996).
[3] L. Pefiti, in idem Ref. [2].
[4] Y. Kantor, M. Kardar, and D. R. Nelson, Phys. Rev. Lett. **57**, 791 (1986); Phys. Rev. A **36**, 3056 (1987).
[5] D. R. Nelson and L. Peliti, J. Phys. (France) **48**, 1085 (1987).
[6] M. Paczuski, M. Kardar, and D. R. Nelson, Phys. Rev. Lett. **60**, 2638 (1988).
[7] F. David and E. Guitter, Europhys. Lett. **5**, 709 (1988).
[8] J. Aronovitz and T. Lubensky, Phys. Rev. Lett. **60**, 2636 (1988).
[9] J. Aronovitz, L. Golubovic, and T. Lubensky, J. Phys. (France) **50**, 609 (1989).
[10] E. Guitter, F. David, S. Leibler, and L. Peliti, Phys. Rev. Lett. **61**, 2949 (1988); J. Phys. (France) **50**, 1787 (1989).
[11] Y. Kantor and D. R. Nelson, Phys. Rev. Lett. **58**, 2774 (1987); Phys. Rev. A **36**, 4020 (1987).
[12] See also M. Baig, D. Espriu, and J. Wheater, Nucl. Phys. B **314**, 587 (1989); R. Renken and J. Kogut, *ibid*. **342**, 753 (1990); R. Harnish and J. Wheater, *ibid*. **350**, 861 (1991).
[13] Y. Kantor and M. V. Jarić, Europhys. Lett. **11**, 157 (1990).
[14] P. Di Francesco and E. Guitter, Europhys. Lett. **26**, 455 (1994).
[15] P. Di Francesco and E. Guitter, Phys. Rev. E **50**, 4418 (1994).
[16] E. N. M. Cirillo, G. Gonnella, and A. Pelizzola, Phys. Rev. E **53**, 1479 (1996).
[17] M. Bowick, P. Di Francesco, O. Golinelli, and E. Guitter, Nucl. Phys. B **450**, 463 (1995).
[18] E. N. M. Cirillo, G. Gonnella, and A. Pelizzola, Phys. Rev. E **53**, 3253 (1996).
[19] See also A. E. Lobkovsky, S. Gentges, Hao Li, D. Morse, and T. A. Witten, Science **270**, 1482 (1995); E. M. Kramer and A. E. Lobkovsky, Phys. Rev. E **53**, 1465 (1996); A. E. Lobkovsky, *ibid*. **53**, 3750 (1996).
[20] D. C. Mattis, Phys. Lett. **56A**, 421 (1976); **60**, 492(E) (1977).
[21] R. Kikuchi, J. Chem. Phys. **60**, 1071 (1974).
[22] T. Morita, Prog. Theor. Phys. **103**, 103 (1984).
[23] C. Buzano, A. Maritan, and A. Pelizzola, J. Phys. Condens. Matter **6**, 327 (1994).
[24] S. F. Edwards and P. W. Anderson, J. Phys. F **5**, 965 (1975).
[25] G. An, J. Stat. Phys. **52**, 727 (1988).
[26] T. Morita, J. Stat. Phys. **59**, 819 (1990).
[27] D. Bensimon, D. Mukamel, and L. Peliti, Europhys. Lett. **18**, 269 (1992).
[28] R. Attal, S. Chaieb, and D. Bensimon, Phys. Rev. E **48**, 2232 (1993).